Active scaffolds for on-demand drug and cell delivery

Xuanhe Zhao[a,b], Jaeyun Kim[b], Christine A. Cezar[b], Nathaniel Huebsch[b,c], Kangwon Lee[b], Kamal Bouhadir[d], and David J. Mooney[b,1]

[a]Soft Active Materials Laboratory, Department of Mechanical Engineering and Materials Science, Duke University, Durham, NC 27708; [b]School of Engineering and Applied Sciences and Wyss Institute, Harvard University, Cambridge, MA 02139; [c]Harvard-Massachusetts Institute of Technology Division of Health Sciences and Technology, Cambridge, MA 02139; and [d]Department of Chemistry, American University of Beirut, Beirut 11-0236, Lebanon

Edited by Alexander M. Klibanov, Massachusetts Institute of Technology, Cambridge, MA, and approved November 11, 2010 (received for review June 4, 2010)

Porous biomaterials have been widely used as scaffolds in tissue engineering and cell-based therapies. The release of biological agents from conventional porous scaffolds is typically governed by molecular diffusion, material degradation, and cell migration, which do not allow for dynamic external regulation. We present a new active porous scaffold that can be remotely controlled by a magnetic field to deliver various biological agents on demand. The active porous scaffold, in the form of a macroporous ferrogel, gives a large deformation and volume change of over 70% under a moderate magnetic field. The deformation and volume variation allows a new mechanism to trigger and enhance the release of various drugs including mitoxantrone, plasmid DNA, and a chemokine from the scaffold. The porous scaffold can also act as a depot of various cells, whose release can be controlled by external magnetic fields.

cell therapy | tissue regeneration | controlled delivery | stimuli responsive | magnetomechanics

For over two decades, porous biomaterials fabricated from natural and synthetic polymers, metals, ceramics, and glasses have been intensively studied and widely used as drug delivery vehicles and scaffolds for tissue regeneration (1–5). For example, collagen sponges that release bone morphogenetic proteins are widely used in spine surgery, with an approximately billion-dollar market (6). The porous scaffolds provide a three-dimensional environment that preserves tissue volume, supports cell interactions, and delivers biological agents (7–10). More recently, porous scaffolds have shown great promise as carriers in cell therapy in the treatment of a variety of diseases (11–14). Significant improvement in cell viability, engraftment, and control over cell fate is possible by delivering cells with the porous scaffolds, in contrast to cell injections or infusions (15–17). In all these cases, it is highly desirable to trigger and/or regulate the delivery of biological agents (e.g., drugs and cells) with external cues, because dynamical control over delivery can potentially improve the safety and efficiency of the agents, and permit new therapies (18). In the field of drug delivery, active biomaterials that are responsive to external stimuli such as temperature, pH, enzymes, and various physical fields have been extensively explored for controlled delivery (19–24). On the other hand, the porous scaffolds currently used in tissue engineering and cell therapy are mostly passive in that they deliver biological agents mainly through mechanisms involving molecular diffusion, material degradation, and cell migration, which do not allow for dynamic external regulations. We believe that *active porous scaffolds* capable of delivering biological agents under the controls of external stimuli can be achieved by appropriate design and tailoring of porous biomaterials (25).

Here, we demonstrate an active scaffold in the form of a macroporous ferrogel, which is responsive to magnetic fields. Ferrogels consisting of magnetic particles embedded in polymer gels have been intensively investigated, due to the broad application and clinical acceptance of magnetic particles and magnetic fields (26–31). Recent studies have shown controlled release of a number of drugs from ferrogels subject to magnetic fields (32–37). Ferrogels have also been made biodegradable (38) and injectable (39). However, typical ferrogels for drug delivery demonstrate very limited deformation and volumetric change, and the pore sizes in most ferrogels are in the nanometer range (36), which limits transport of large molecules and cells through the gels. Cell delivery from ferrogels is particularly difficult, and the polymers typically used to fabricate ferrogels do not support cell adhesion (33, 37). To create the magnetic-sensitive scaffolds capable of on-demand drug and cell delivery in the current study, polymer gels were fabricated with three-dimensionally connected macropores and coupled with magnetic nanoparticles and cell-binding peptides. Alginate, a naturally occurring polysaccharide, which comprises α-L-guluronic and β-D-mannuronic acid sugar residues, was used to fabricate the scaffolds, because it had been used extensively in biomedical applications. Peptides containing the arginine-glycine-aspartic acid (RGD) amino acid sequence, a ubiquitous cell-binding domain found in many extracellular matrix molecules, were covalently coupled to the alginate. Iron oxide particles with diameters ∼10 nm were embedded in the alginate, which results in a superparamagnetic gel (39). Macroporous structures with interconnected pores in the micrometer range were generated from the gels. Under applied magnetic fields, the macroporous ferrogel can give large and prompt deformation, causing water flow through the interconnected pores. The deformation and water convection can trigger and enhance release of biological agents. Various drugs and cells were encapsulated in the scaffolds, and their ability to be released under the control of external magnetic fields was probed in vitro and in vivo.

Results

Macroporous ferrogels were first developed to allow for bioactive agents ranging from molecules to cells to be encapsulated and released on demand. Macroporous gels with a hierarchal structure (Fig. 1) of various sizes (millimeter to centimeter or larger) and shapes (Fig. 1*A*) can readily be fabricated to accommodate specific applications. Pores with controlled sizes and connectivity were introduced into the ferrogels by freezing gels at different temperatures prior to lyophilization (40). Corresponding to freezing temperatures of −20, −80, and −180 °C, the average diameters of the pores were 700, 300, and 20 μm. Highly interconnected pores were observed in gels prepared at −20 and −80 °C, whereas poorly interconnected pores were observed in gels prepared at −180 °C (Fig. S1 and Movies S1, S2, and S3). This finding agrees with the earlier reports on alginate macroporous gels (40, 41). Highly monodisperse iron oxide nanoparticles with a diameter ∼10 nm were embedded in the gel at predetermined concentrations (Fig. 1*C*, *Left*, 13 wt %; *Right*, 4 wt %) (42). The surfaces of the nanoparticles were precoated with Pluronic F127 (Fig. 1*D*) (43) to minimize agglomeration, which resulted in a relatively homogeneous distribution of nanoparticles in the gels.

Author contributions: X.Z. and D.J.M. designed research; X.Z., J.K., C.A.C., N.H., K.L., and K.B. performed research; X.Z., J.K., C.A.C., N.H., K.L., and D.J.M. analyzed data; and X.Z. and D.J.M. wrote the paper.

The authors declare no conflict of interest.

This article is a PNAS Direct Submission.

[1]To whom correspondence should be addressed. E-mail: mooneyd@seas.harvard.edu.

This article contains supporting information online at www.pnas.org/lookup/suppl/doi:10.1073/pnas.1007862108/-/DCSupplemental.

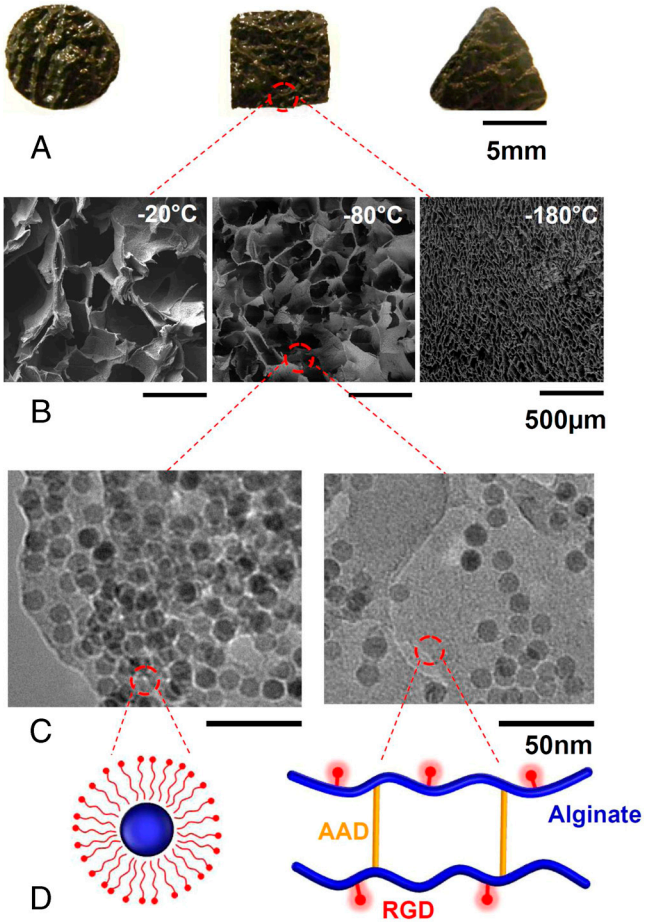

Fig. 1. The hierarchical structure of macroporous ferrogels. (*A*) Photograph of bulk gels with various shapes. (*B*) SEM images of scaffold with various pore sizes (average diameter from left to right: 700, 300, and 20 μm) and pore connectivity (from left to right: good, good, poor) in the ferrogels. (*C*) Transmission electron microscope images of iron oxide nanoparticles in the gel at predetermined concentrations (*Left*, 13 wt %; *Right*, 4 wt %). (*D*) Schematic plots of the nanoparticles coated with Pluronic F127 (*Left*) and alginate covalently cross-linked by AAD and coupled with RGD peptides (*Right*). Size bars are shown on images.

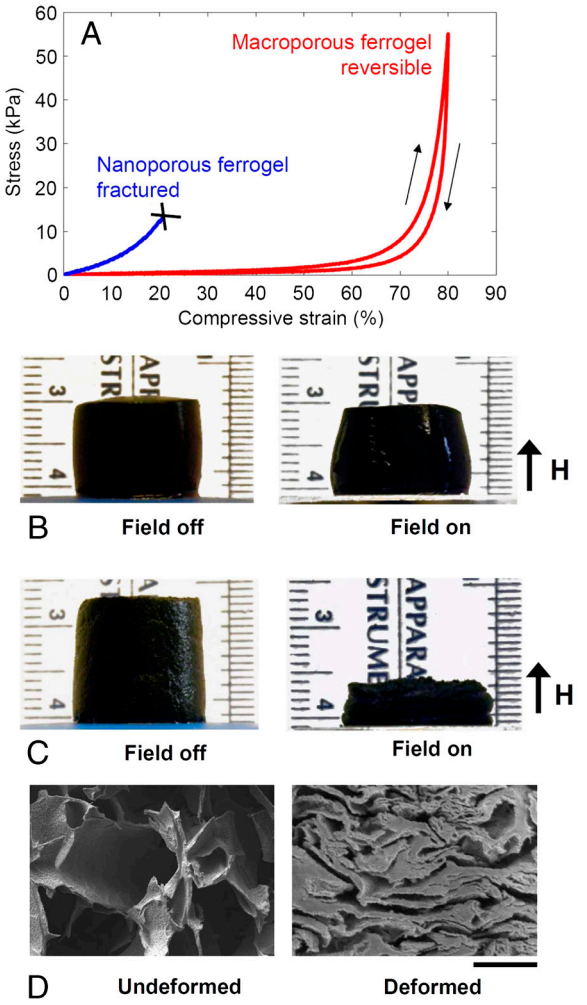

Fig. 2. (*A*) Stress vs. strain curves for nanoporous ferrogel and macroporous ferrogel subjected to compression tests. (*B*) A cylinder of a nanoporous ferrogel reduced its height ~5% when subjected to a vertical magnetic-field gradient of ~38 A/m^2. (*C*) The corresponding macroporous ferrogel deformed ~70% under the same magnetic field. (*D*) SEM images of a freeze-dried macroporous ferrogel in the undeformed and deformed states. (Scale bar: 500 μm.)

Alginate gels were covalently cross-linked with adipic acid dihydrazide (AAD) (Fig. 1*D*) (40), because the covalent cross-links allowed gels to maintain the macroporous structure following lyophilization and subsequent rehydration. Peptides containing the RGD amino acid sequence were covalently coupled to the polymer prior to gel formation (Fig. 1*D*) (44).The RGD coupling confers a specific mechanism for integrin-mediated cell adhesion to the otherwise nonadhesive polymer, and the RGD density can be manipulated to provide control over cell adhesion.

The influence of the macropores on the gel mechanical properties were next evaluated because the stiffness of the gels will dictate the extent of deformation that will result from a specific magnetic field. It is well established that by creating pores in a gel, one can greatly reduce its elastic rigidity (45). A ferrogel fabricated with 13 wt % Fe_3O_4 and 1 wt % alginate cross-linked by 5 mM AAD gives an initial Young's modulus (i.e., the slope of the initial part of the stress vs. strain curve in Fig. 2*A*) of ~30 kPa in a compression test. Introducing connected pores of ~700-μm diameter into the ferrogel led to a dramatic reduction in the initial modulus, to ~2.5 kPa (Fig. 2*A*). These macroporous gels can also be reversibly deformed to a compressive strain of over 80% before fracture, in contrast to the more brittle nature of the standard nanoporous alginate gels (Fig. 2*A*). In addition, it has been observed that the initial Young's modulus of the macroporous gel decreases with the rise of the freezing temperature used in preparation of the gel (Fig. S2). Macroporous ferrogels fabricated with 13 wt % Fe_3O_4 and 1 wt % alginate cross-linked by 5 mM AAD, and frozen at −20 °C were used for the remaining experiments. The macroporous ferrogels with interconnected pores, larger pore size (Fig. 1*B*), higher concentration of iron oxide particles (Fig. 1*C*), and lower modulus (Fig. S2) were chosen because (*i*) drug and cell transport will presumably be more efficient in scaffolds with larger pore sizes and better connectivity (40), (*ii*) a higher iron-oxide-particle density gives a higher body force under the same magnetic field, and (*iii*) a gel with lower modulus tends to deform more when subject to the same body forces. Large deformation of the gel leads to more pronounced effects on drug and cell release.

The deformation of nanoporous and macroporous ferrogels under the influence of a moderate magnetic field was next examined. Subject to a nonuniform magnetic field, a ferrogel experiences a body force proportional to the gradient of the applied field, which results in a shape change (46, 47). A cylinder of a typical nanoporous ferrogel reduced its height by ~5% when subjected to a vertical magnetic-field gradient of ~38 A/m^2, using a magnetic bar placed at the bottom of the gel (Fig. 2*B*). In comparison, a cylinder of the macroporous ferrogel gives a much

larger deformation, ~70%, under the same magnetic field (Fig. 2*C*), due to its lower modulus and the increase of iron-oxide-particle density during deformation (Fig. 2*A*). In addition, the cylinder of the macroporous gel also reduced its volume by ~70% (Fig. 2*C*), as contrasted to a minimal volume change of the nanoporous gels (Fig. 2*B*). The large volume change of the macroporous gels was caused by collapse of the pores in these gels, as demonstrated by SEM images of freeze-dried macroporous ferrogels in the deformed and undeformed states (Fig. 2*D*). The collapsing pores will force water contained in the connected pores to flow out of the gel. Once the magnetic field is off, the elastically deformed gel quickly returns to its original, undeformed configuration in less than 1 s, as surrounding water was reabsorbed into the gel (Movie S4).

We hypothesized that the magnetic-field-induced gel deformation and resulting water convection and associated shear forces could accelerate the release of drugs encapsulated in ferrogels or cells adherent to the pore surfaces of the macroporous ferrogels. To test this hypothesis, we first chose mitoxantrone (M_r 444 444), an antineoplastic agent, as a model drug. Mitoxantrone forms an ionic complex with the carboxylate groups on alginate, which retards its release (48). Macroporous ferrogels each containing 300 mg mitoxantrone were placed in a PBS solution. Every 30 min, one group of the macroporous ferrogels was subjected to 120 cycles (on/off) of the magnetic field over 2 min by manually approaching and retracting a magnet against the gels, while no magnetic field was applied to the other gels. The short recovery time of the gels allows them to recover their initial dimensions in each cycle. Gel deformation and water convection promotes dissociation of drugs from the polymer and enhances transport of unbound drugs out of the gel. The macroporous gel deformed reversibly and promptly in response to the cycling magnetic field, and the applied magnetic stimulation greatly accelerated the release of mitoxantrone, as shown grossly by the increasing blue color in the PBS. (see Movie S2). The cumulative release profile showed a stepwise increment with magnetic stimulation, and the total amount of mitoxantrone released from the stimulated gel was ~7 times more than that of the control case after 3 h (Fig. 3*A*). This study was repeated with higher molecular-weight biological agents, plasmid DNA ($M_r \sim 10^6$) condensed with polyethyleneimine (PEI, $M_r \sim 22{,}000$), and the chemokine SDF-1α (M_r 8,000) to determine if this approach would have utility with a wide range of potential drugs. Again, significant stepwise increases in release were noted with application of the magnetic field, as compared to control gels (Fig. 3 *B* and *C*).

Next, we used the macroporous ferrogel to examine controlled cell release in vitro (Fig. 4*A*). The RGD on alginate in macroporous ferrogels enables cells to adhere on the porous surfaces and the adhesion strength increases with RGD density (49). A baseline RGD density was set to 7.43 μmol RGD per gram of alginate (50), and 50% and 10% of the baseline RGD density were also used to examine the role of gel adhesiveness on cell release. Human dermal fibroblasts (1.5×10^6) were seeded in each gel, and gels were incubated at 37 °C for 4 h to allow cell adhesion. Thereafter, the macroporous ferrogels were subject to 120 cycles (on/off) of the magnetic field for ~2 min, at 2-h intervals. The cumulative release of cells was quantified as a function of time (Fig. 4*B*). Magnetic stimulation resulted in burst release of cells and the release profile varied for gels with different RGD densities. After 6 h (three rounds of magnetic stimulation), around a third of the cells were released from gels with the baseline RGD density, while over half of the cells were released from ferrogels with 50% less RGD. The gels with only 10% of the baseline RGD content delivered over 90% of their cells after 4 h (two rounds of stimulation). These results are consistent with the lower RGD densities providing weaker cell adhesion, resulting in more cell detachment and release under the magnetic stimulation (51). The released cells were collected and probed for viability. More

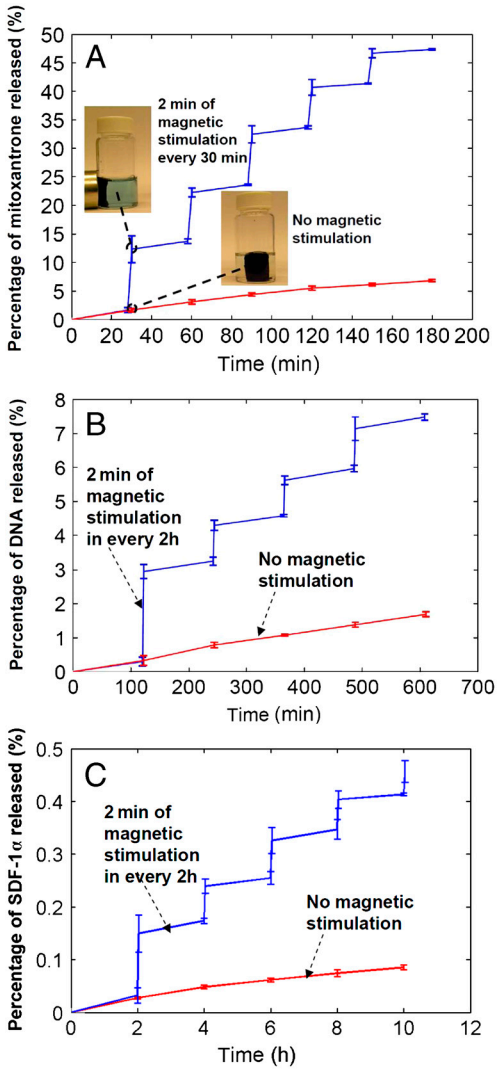

Fig. 3. (*A*) Cumulative release profiles of mitoxantrone from macroporous ferrogels subject to 2 min of magnetic stimulation every 30 min, or no magnetic stimulation. (*B*) Cumulative release profiles of plasmid DNA from macroprous ferrogels subject to 2 min of magnetic stimulation every 2 h or no magnetic stimulation. (*C*) Cumulative release profiles of SDF-1α from macroporous ferrogels subject to 2 min of magnetic stimulation every 2 h or no magnetic stimulation. Values represent mean and standard deviation of each increment ($n = 3$–5).

than 95% of the released cells were viable (Fig. S3). The released cells were also incubated in a Petri dish at 37 °C. These cells spread normally and became confluent after 2 d (Fig. 4*C*), indicating that released cells remained viable and functional.

Finally, we examined the capability of macroporous ferrogels in controlled delivery of cells in vivo. Mouse mesenchymal stem cells (1.5×10^6) stained with DiOC18, a membrane dye with near infrared emission maximum, were seeded in macroporous ferrogels with 50% baseline RGD content. The gels were implanted into the subcutaneous space of mice. One hour after the implantation, the gels were subjected to 120 cycles (on/off) of the external magnetic field by approaching and retracting a magnet against the mouse skin over the gel. As a control, implanted ferrogels were subject to no magnetic stimulation, and in vivo fluorescence images of both conditions were obtained before and after magnetic stimulation (Fig. 5). The control mouse (Fig. 5 *A* and *B*, *Left*) showed almost no change in fluorescence, indicating few cells were released from the ferrogel. In contrast, application of the external magnetic field led to a significant increase in

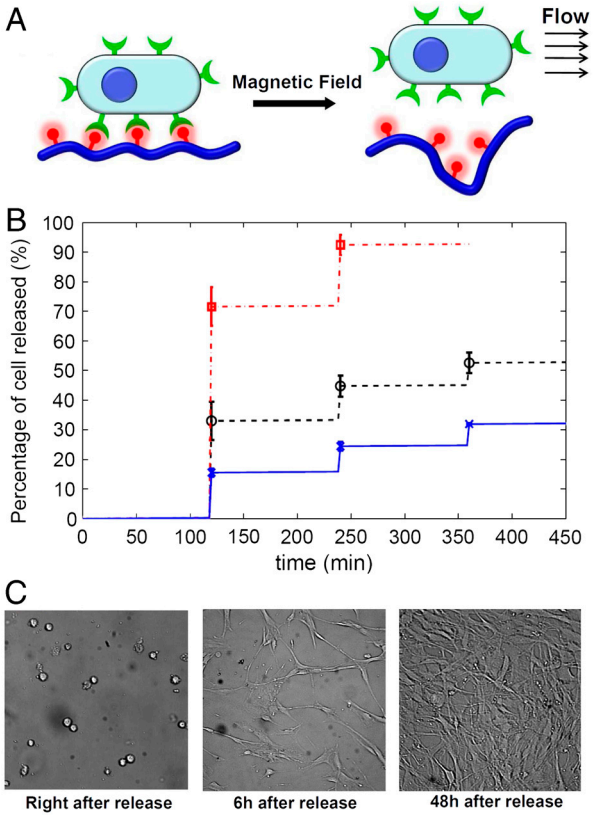

Fig. 4. (*A*) Schematic plot of gel deformation and resulting water convection inducing cell release from macroporous gels (51). (*B*) Cumulative release profiles of fibroblasts from macroporous ferrogels with 100% (cross), 50% (circle), and 10% (square) of the baseline RGD density, following application of cycled magnetic field. (*C*) Spreading and proliferation of the released cells at various times after replating onto tissue culture plastic. Values in *B* represent mean and standard deviation of each increment ($n = 3$–5). Differences between the values of cell release at the various RGD densities were statistically significant at each time point ($p < 0.05$).

fluorescence around the ferrogel, indicating a burst release of stem cells.

Discussion

The results of this study suggest an on-demand and reversible approach for delivering various biological agents from a newly designed macroporous ferrogel, in response to external magnetic fields. A delivery mechanism, based on deformation of macroporous ferrogels under magnetic stimulation, and subsequent water flow through connected pores is demonstrated. By creating large pores in a ferrogel, one can greatly reduce the rigidity of the gel and increase its hydraulic conductivity (45). As a result, the macroporous ferrogels demonstrate very large deformation, volumetric change, and water convection under applied magnetic fields, in contrast to the minimal values of conventional nanoporous ferrogels. Furthermore, it is generally difficult for nanoporous ferrogels to release drugs with high molecular weight, such as proteins and plasmid DNA, due to the limited mobility of these drugs in the nanopores (32–37). The connected macropores in the new ferrogel enable the rapid transport of various drugs ranging from small molecules such as mitoxantrone to very large molecules such as the protein SDF-1α and plasmid DNA out of the gel, upon magnetic stimulation. This result is consistent with previous observations that mechanical compression of macroporous or nanoprous gels can enhance the release of biological agents (51, 52). Here, we further demonstrated that reversible deformation of macroporous ferrogels allows a mechanism for on-demand drug and cell release under the control of external magnetic fields.

These scaffolds also act as active depots of various cells whose release can be controlled over time. The polymers used to form conventional ferrogels typically do not support cell adhesion (33, 37). To address this issue, the polymer used to form the ferrogels in this study was covalently coupled with cell-binding peptides because the peptide density can be manipulated to provide control over cell adhesion. On-demand release of human dermal fibroblasts and mouse mesenchymal stem cells were demonstrated in vitro and in vivo under the control of external magnetic fields. The peptide-modified macroporous ferrogel also maintains the adhesion and viability of the resident cells, and subjecting the gels to external magnetic stimulation allows one to release a prescribed number of the resident cells on demand over various time frames. Multiple parameters in this delivery system are tunable, including peptide density, the strength of applied magnetic field, number of magnetic cycles, and frequency of magnetic stimulation, to control the release of various cell types. This on-demand release of cells from porous scaffolds is potentially of wide utility for tissue regeneration and cell therapies. The current study has been focused on the capability of active porous scaffolds in on-demand drug and cell deliveries, but we also expect these macroporous ferrogels to find broader applications, including serving as actuators and sensors in biomedical and other applications, due to their large and fast deformation and volume change under magnetic fields.

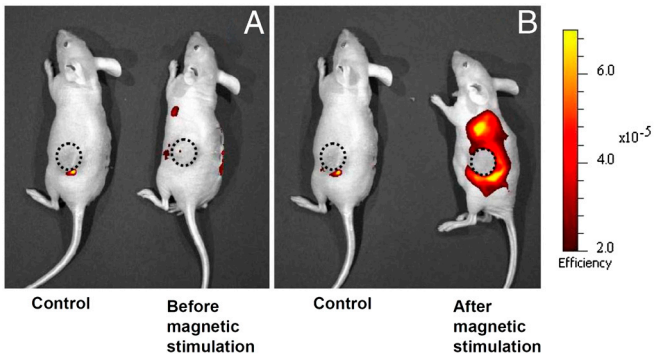

Fig. 5. In vivo fluorescence images of mice implanted with macroporous ferrogels containing mouse mesenchymal stem cells stained with DiOC18 before (*A*) and after (*B*) magnetic stimulation. The control case was subject to no magnetic stimulation. The positions of the gel disks are indicated by circles on the figure.

Materials and Methods

Materials. Sodium alginate with high guluronate content (Protanal LF 20/60) was purchased from Pronova Biopolymers, Inc. and used without further purification. PBS was purchased from Invitrogen. AAD, 1-ethyl-3-(dimethylaminopropyl) carbodiimide (EDC), MES, 1-hydroxybenzotriazole (HOBt), Iron(III) chloride hexahydrate, oleic acid, 1-octadecene, and cetyltrimethylammonium bromide were purchased from Sigma-Aldrich. Sodium oleate was purchased from TCI. Pluronic F127 was purchased from BASF. The integrin-binding peptide $(Gly)_4$-Arg-Gly-Asp-Ala-Ser-Ser-Lys-Tyr was purchased from Commonwealth Biotech.

Macroporous Ferrogel Fabrication. The Fe_3O_4 nanoparticles were fabricated according to ref. 42 and the surfactant, Pluronic F127, was coated on the nanoparticles following the procedure in ref. 43. Alginates were coupled with RGD following aqueous carbodiimide chemistry as described in ref. 44. To prepare macroporous ferrogels, RGD-modified alginate in MES buffer (0.1 M MES and 0.5 M NaCl, pH 6.0) was sequentially mixed with an aqueous solution of Fe_3O_4 nanoparticles, HOBt, EDC, and AAD. The concentration of alginate was 1 wt %, Fe_3O_4 nanoparticles was 13 wt %, and AAD was 5 mM in the resulting solution. A baseline RGD density was set to 7.43 μmol RGD per gram of alginate according to ref. 50. The mixture was immediately cast between two glass plates separated by 4 ~ 11-mm

spacers. After 2 h, the ferrogel was cut into various shapes and placed in a large volume of distilled water, for a minimum of 24 h, to remove any residual reagents. The gels were then frozen at −20, −80, or −180 °C and lyophilized to generate macroporous ferrogels with variable pore characteristics.

SEM Sample Preparation. The SEM samples in Fig. 1*B* were prepared by sectioning the as-prepared macroporous ferrogels before hydration in water. To prepare the SEM samples in Fig. 2*D*, hydrated macroporous ferrogels were frozen in the undeformed and deformed states in liquid nitrogen, and then lyophilized and sectioned for observation.

Pore Size and Connectivity Evaluation. The average sizes of the pores in macroporous gels were calculated by averaging the diameters of the pores in the gels observed by SEM. To assess the pore connectivity, the gels were soaked in a solution containing 1.0×10^8/mL FluoSpheres red fluorescent microspheres (Molecular Probes) with 1-μm diameter and subject to 120 cycles (on/off) of the external magnetic field. The gels were then dehydrated and examined using microcomputed tomography (mirco-CT) to determine the distribution of the fluorescent beads within the gels. Micro-CT images visualized were obtained from the midplane (2.5-mm above the bottom of gels) of the cylindrical-shaped ferrogel scaffolds (5 mm in height). Fluorescent beads were imaged at high resolution (HMXST225, X-Tek; Nikon Metrology NV) with the scanner set to a voltage of 100 kV and a current of 100 A. Next, a series of 2D images of each sample was taken with an X-Tek X-ray machine while the sample was rotated 360°. The series of 2D images were converted to 3D images using CT Pro software. Image rendering and subsequent image processing including movie production were performed with Volume Graphics studio MAX. The pore connectivity was further evaluated using a water wicking technique in which the interconnected porosity was calculated as the interconnected void volume over the total volume. To determine total volume, gels were soaked in water for 1 h and weighed. A Kimwipe was then used to wick away water within interconnected pores and the gels were weighed once again. The interconnected void volume was calculated as the volume of water wicked from the gels.

Mechanical Testing. The nanoporous ferrogel and macroporous ferrogel were cut into cylinders (15-mm diameter, 8-mm height). The cylinders were subject to compression tests using an Instron 3342 from Instron with a strain rate of 20% per minute. Engineering stresses and strains were recorded. The ferrogel cylinders were kept hydrated throughout the tests.

Controlled Release of Mitroxantrone. The macroporous ferrogels in dry state were cut into disks with a volume ∼2 mL. Each disk was allowed to absorb 1 mL of an aqueous solution of mitoxantrone with a concentration of 300 mg/mL. The resulting gels were stored at room temperature for ∼6 h. The macroporous ferrogels were then placed in a PBS solution. Every 30 min, one group of the macroporous ferrogels was subjected to 120 cycles (on/off) of the magnetic field over 2 min, while no magnetic field was applied to the other gels. The medium surrounding each disk was collected and replaced with fresh buffer every 30 min and after each period of magnetic stimulation. Mitoxantrone concentration was recorded by measuring the absorbance of mitroxantrone in PBS solution at a wavelength of 327.5 nm.

Controlled Release of Plasmid DNA. Plasmid DNA (Aldevron) was combined with linear PEI (Fermentas) to form a polyelectrolyte complex as described in ref. 53. The ratio of the number of amine groups in PEI to the number of phosphate groups (N/P ratio) in DNA was kept constant at 7. Macroporous ferrogels with a volume ∼1 mL were allowed to absorb 0.5 mL of an aqueous solution of plasmid DNA-PEI complex with a DNA concentration of 600 μg/mL. Thereafter, ferrogel disks were used for the release study following a similar procedure as described in controlled release of mitroxantrone, except the magnetic field was applied every 2 h instead of every 30 min. The medium surrounding each disk was collected and replaced with fresh buffer every 2 h and after each period of magnetic stimulation. The concentration of plasmid DNA released into the medium was measured using Quant-iT™ PicoGreen® dsDNA Assay Kit (Invitrogen).

Controlled Release of SDF-1α. Macroporous ferrogels with a volume ∼1 mL were allowed to absorb 0.5 mL of an aqueous solution of human SDF-1α (PeproTech) with a concentration of 2 μg/mL. Ferrogel disks were used for the release study following a procedure similar to that described in the controlled release of mitroxantrone, except the magnetic field was applied every 2 h instead of every 30 min. The medium surrounding each disk was collected and replaced with fresh buffer every 2 h and after each period of magnetic stimulation. SDF-1α protein concentrations were then determined using an Enzyme Linked Immunosorbent Assay Kit for human SDF-1α (R&D Systems).

Controlled Cell Release in Vitro. Human dermal fibroblasts (1.5×10^6) (Lonza) were seeded in each ferrogel gel disk, and the gel disks were incubated at 37 °C for 4 h to allow cell adhesion. Thereafter, the ferrogel disks were placed in FBS-supplemented DMEM and the cells were released following a similar procedure as described in controlled release of mitroxantrone, except the magnetic field was applied every 2 h instead of every 30 min. The medium surrounding each disk was collected and replaced with fresh DMEM every 2 h and after each period of magnetic stimulation. The numbers of cells released were counted with a Z2™ Coulter Counter (Beckman Coulter). The cells released by magnetic stimulation were also incubated in a Petri dish with DMEM at 37 °C to monitor adhesion and proliferation.

Controlled Cell Release in Vivo. Mouse mesenchymal stem cells (1.5×10^6) (ATCC) stained with DiOC18 (Invitrogen) according to manufacturer's protocol were seeded in each ferrogel gel disk, and the gel disks were incubated at 37 °C for 4 h to allow cell adhesion. The gel disks were implanted subcutaneously into the back region of female nude mice (NU/J, Jackson Laboratory) under anesthesia, and the incisions were closed by 5-0 Ethilon sutures (Johnson & Johnson). In order to create a space for placement of gels and cell release, liquid pockets were generated around the ferrogels by subcutaneous PBS injection prior to gel placement. One hour after the implantation, the ferrogels were subject to 120 cycles (on/off) of the external magnetic field by approaching and retracting a magnet against the skin of the mouse. Fluorescence images of mice were obtained on a Xenogen IVIS Spectrum system (Caliper Life Sciences). Animal work was performed in compliance with National Institutes of Health and institutional guidelines.

ACKNOWLEDGMENTS. This work was supported by the Materials Research Science and Engineering Center at Harvard University, National Institutes of Health/National Institute of Dental and Craniofacial Research Grant (R01 DE019917), the BASF research initiative at Harvard University, and the Defense Advanced Research Projects Agency (W911NF-10-0113). X.Z. acknowledges the startup funds from the Pratt School of Engineering at Duke University.

1. Langer R, Vacanti JP (1993) Tissue engineering. *Science* 260:920–926.
2. Griffith LG, Naughton G (2002) Tissue engineering—current challenges and expanding opportunities. *Science* 295:1009–1016.
3. Hutmacher DW (2000) Scaffolds in tissue engineering bone and cartilage. *Biomaterials* 21:2529–2543.
4. Karageorgiou V, Kaplan D (2005) Porosity of 3D biornaterial scaffolds and osteogenesis. *Biomaterials* 26:5474–5491.
5. Hollister SJ (2005) Porous scaffold design for tissue engineering. *Nat Mater* 4:518–524.
6. Mroz T, Yamashita T, Lieberman I (2008) The on- and off-label use of rhBMP-2 (INFUSE) in Medicare and non-Medicare patients. *Spine J* 8:41S–42S.
7. Mikos AG, et al. (1994) Preparation and characterization of poly(L-lactic acid) foams. *Polymer* 35:1068–1077.
8. Mooney DJ, Baldwin DF, Suh NP, Vacanti LP, Langer R (1996) Novel approach to fabricate porous sponges of poly(D,L-lactic-co-glycolic acid) without the use of organic solvents. *Biomaterials* 17:1417–1422.
9. Shastri VP, Martin I, Langer R (2000) Macroporous polymer foams by hydrocarbon templating. *Proc Natl Acad Sci USA* 97:1970–1975.
10. Yang SF, Leong KF, Du ZH, Chua CK (2001) The design of scaffolds for use in tissue engineering. Part 1. Traditional factors. *Tissue Eng* 7:679–689.
11. Hofmann M, et al. (2005) Monitoring of bone marrow cell homing into the infarcted human myocardium. *Circulation* 111:2198–2202.
12. Skuk D, Caron NJ, Goulet M, Roy B, Tremblay JP (2003) Resetting the problem of cell death following muscle-derived cell transplantation: Detection, dynamics and mechanisms. *J Neuropathol Exp Neurol* 62:951–967.
13. Evans SM, Mummery C, Doevendans PA (2007) Progenitor cells for cardiac repair. *Semin Cell Dev Biol* 18:153–160.
14. Thuret S, Moon LDF, Gage FH (2006) Therapeutic interventions after spinal cord injury. *Nat Rev Neurosci* 7:628–643.
15. Auger FA, Berthod F, Moulin W, Pouliot R, Germain L (2004) Tissue-engineered skin substitutes: From in vitro constructs to in vivo applications. *Biotechnol Appl Biochem* 39:263–275.
16. Nerem RM (2007) Cell-based therapies: From basic biology to replacement, repair, and regeneration. *Biomaterials* 28:5074–5077.
17. Mooney DJ, Vandenburgh H (2008) Cell delivery mechanisms for tissue repair. *Cell Stem Cell* 2:205–213.
18. Langer R (1990) New methods of drug delivery. *Science* 249:1527–1533.
19. Hoffman AS (1995) Intelligent polymers in medicine and biotechnology. *Artif Organs* 19:458–467.

20. Hsieh DST, Langer R, Folkman J (1981) Magnetic modulation of release of macromolecules from polymers. *Proc Natl Acad Sci USA* 78:1863–1867.
21. Peppas NA, Hilt JZ, Khademhosseini A, Langer R (2006) Hydrogels in biology and medicine: From molecular principles to bionanotechnology. *Adv Mater* 18:1345–1360.
22. Galaev IY, Mattiasson B (1999) 'Smart' polymers and what they could do in biotechnology and medicine. *Trends Biotechnol* 17:335–340.
23. Miyata T, Asami N, Uragami T (1999) A reversibly antigen-responsive hydrogel. *Nature* 399:766–769.
24. Wood KC, et al. (2008) Electroactive controlled release thin films. *Proc Natl Acad Sci USA* 105:2280–2285.
25. Mitragotri S, Lahann J (2009) Physical approaches to biomaterial design. *Nat Mater* 8:15–23.
26. Weissleder R, Bogdanov A, Neuwelt EA, Papisov M (1995) Long-circulating iron-oxides for Mr-imaging. *Adv Drug Delivery Rev* 16:321–334.
27. Brigger I, Dubernet C, Couvreur P (2002) Nanoparticles in cancer therapy and diagnosis. *Adv Drug Delivery Rev* 54:631–651.
28. Lu AH, Salabas EL, Schuth F (2007) Magnetic nanoparticles: Synthesis, protection, functionalization, and application. *Angew Chem, Int Ed* 46:1222–1244.
29. Gupta AK, Gupta M (2005) Synthesis and surface engineering of iron oxide nanoparticles for biomedical applications. *Biomaterials* 26:3995–4021.
30. Pankhurst QA, Connolly J, Jones SK, Dobson J (2003) Applications of magnetic nanoparticles in biomedicine. *J Phys D Appl Phys* 36:R167–R181.
31. Mornet S, Vasseur S, Grasset F, Duguet E (2004) Magnetic nanoparticle design for medical diagnosis and therapy. *J Mater Chem* 14:2161–2175.
32. Lu ZH, et al. (2005) Magnetic switch of permeability for polyelectrolyte microcapsules embedded with Co@Au nanoparticles. *Langmuir* 21:2042–2050.
33. Hu SH, Liu TY, Liu DM, Chen SY (2007) Controlled pulsatile drug release from a ferrogel by a high-frequency magnetic field. *Macromolecules* 40:6786–6788.
34. Hu SH, Chen SY, Liu DM, Hsiao CS (2008) Core/single-crystal-shell nanospheres for controlled drug release via a magnetically triggered rupturing mechanism. *Adv Mater* 20:2690–2695.
35. Liu TY, Hu SH, Liu TY, Liu DM, Chen SY (2006) Magnetic-sensitive behavior of intelligent ferrogels for controlled release of drug. *Langmuir* 22:5974–5978.
36. Hu SH, Liu TY, Liu DM, Chen SY (2007) Nano-ferrosponges for controlled drug release. *J Controlled Release* 121:181–189.
37. Resendiz-Hernandez PJ, Rodriguez-Fernandez OS, Garcia-Cerda LA (2008) Synthesis of poly(vinyl alcohol)-magnetite ferrogel obtained by freezing-thawing technique. *J Magn Magn Mater* 320:E373–E376.
38. Chatterjee J, Haik Y, Chen CJ (2003) Biodegradable magnetic gel: Synthesis and characterization. *Colloid Polym Sci* 281:892–896.
39. Qin J, et al. (2009) Injectable superparamagnetic ferrogels for controlled release of hydrophobic drugs. *Adv Mater* 21:1354–1357.
40. Thornton AJ, Alsberg E, Albertelli M, Mooney DJ (2004) Shape-defining scaffolds for minimally invasive tissue engineering. *Transplantation* 77:1798–1803.
41. Thornton AJ, Alsberg E, Hill EE, Mooney DJ (2004) Shape retaining injectable hydrogels for minimally invasive bulking. *J Urol* 172:763–768.
42. Park J, et al. (2004) Ultra-large-scale syntheses of monodisperse nanocrystals. *Nat Mater* 3:891–895.
43. Qin J, et al. (2007) A high-performance magnetic resonance imaging T-2 contrast agent. *Adv Mater* 19:1874–1878.
44. Drury JL, Mooney DJ (2003) Hydrogels for tissue engineering: Scaffold design variables and applications. *Biomaterials* 24:4337–4351.
45. Gibson LJ, Ashby MF (1997) *Cellular Solids* (Cambridge Univ Press, Cambridge), pp 101–106.
46. Zrinyi M, Barsi L, Buki A (1997) Ferrogel: A new magneto-controlled elastic medium. *Polym Gels Networks* 5:415–427.
47. Zrinyi M, Barsi L, Buki A (1996) Deformation of ferrogels induced by nonuniform magnetic fields. *J Chem Phys* 104:8750–8756.
48. Bouhadir KH, Alsberg E, Mooney DJ (2001) Hydrogels for combination delivery of antineoplastic agents. *Biomaterials* 22:2625–2633.
49. Xiao Y, Truskey GA (1996) Effect of receptor-ligand affinity on the strength of endothelial cell adhesion. *Biophys J* 71:2869–2884.
50. Rowley JA, Madlambayan G, Mooney DJ (1999) Alginate hydrogels as synthetic extracellular matrix materials. *Biomaterials* 20:45–53.
51. Dainiak MB, Kumar A, Galaev IY, Mattiasson B (2006) Detachment of affinity-captured bioparticles by elastic deformation of a macroporous hydrogel. *Proc Natl Acad Sci USA* 103:849–854.
52. Lee KY, Peters MC, Anderson KW, Mooney DJ (2000) Controlled growth factor release from synthetic extracellular matrices. *Nature* 408:998–1000.
53. Kong HJ, Hsiong S, Mooney DJ (2007) Nanoscale cell adhesion ligand presentation regulates nonviral gene delivery and expression. *Nano Lett* 7:161–166.